Computers in Biology and Medicine 165 (2023) 107381

Contents lists available at ScienceDirect

Computers in Biology and Medicine

journal homepage: www.elsevier.com/locate/compbiomed

In silico assessment of the bone regeneration potential of complex porous scaffolds

Reduan Asbai-Ghoudan [a,*], Gabriele Nasello [b], María Ángeles Pérez [c], Stefaan W. Verbruggen [d,e], Sergio Ruiz de Galarreta [a], Naiara Rodriguez-Florez [a,f]

[a] Department of Mechanical Engineering and Materials, Universidad de Navarra, TECNUN Escuela de Ingenieros, Paseo Manuel de Lardizabal, 13, 20018, San Sebastian, Spain
[b] Prometheus Division of Skeletal Tissue Engineering, KU Leuven, O&N1, Herestraat 49, PB 813, 3000, Leuven, Belgium
[c] Multiscale in Mechanical and Biological Engineering, Instituto de Investigación en Ingeniería de Aragón (I3A), Instituto de Investigación Sanitaria Aragón (IIS Aragón), University of Zaragoza, 50018, Zaragoza, Spain
[d] Centre for Bioengineering, School of Engineering and Materials Science, Queen Mary University of London, London, E1 4NS, UK
[e] Department of Mechanical Engineering and INSIGNEO Institute for in Silico Medicine, University of Sheffield, Sheffield, S1 3JD, UK
[f] IKERBASQUE, Basque Foundation for Science, Plaza Euskadi 5, 48009, Bilbao, Spain

ARTICLE INFO

Keywords:
Mechanobiology
Bone regeneration
Scaffolds
Triply periodic minimal surfaces
Mechanical stimulus
FE-Based model

ABSTRACT

Mechanical environment plays a crucial role in regulating bone regeneration in bone defects. Assessing the mechanobiological behavior of patient-specific orthopedic scaffolds in-silico could help guide optimal scaffold designs, as well as intra- and post-operative strategies to enhance bone regeneration and improve implant longevity. Additively manufactured porous scaffolds, and specifically triply periodic minimal surfaces (TPMS), have shown promising structural properties to act as bone substitutes, yet their ability to induce mechanobiologially-driven bone regeneration has not been elucidated. The aim of this study is to i) explore the bone regeneration potential of TPMS scaffolds made of different stiffness biocompatible materials, to ii) analyze the influence of pre-seeding the scaffolds and increasing the post-operative resting period, and to iii) assess the influence of patient-specific parameters, such as age and mechanosensitivity, on outcomes. To perform this study, an *in silico* model of a goat tibia is used. The bone ingrowth within the scaffold pores was simulated with a mechano-driven model of bone regeneration. Results showed that the scaffold's architectural properties affect cellular diffusion and strain distribution, resulting in variations in the regenerated bone volume and distribution. The softer material improved the bone ingrowth. An initial resting period improved the bone ingrowth but not enough to reach the scaffold's core. However, this was achieved with the implantation of a pre-seeded scaffold. Physiological parameters like age and health of the patient also influence the bone regeneration outcome, though to a lesser extent than the scaffold design. This analysis demonstrates the importance of the scaffold's geometry and its material, and highlights the potential of using mechanobiological patient-specific models in the design process for bone substitutes.

1. Introduction

The development of orthopedic implants is focused on guiding bone healing and inspiring innovative solutions in the orthopedic regenerative medicine field [1,2]. Improving implant durability is important to decrease the number of revision procedures and limit healthcare costs [3]. Ulrich et al. [4] reported that out of 225 participants, half needed a revision surgery within 5 years following hip arthroplasty. The most common reason for this prevalence was aseptic loosening, especially in older patients (>50 years-old), covering over 50% of the cases and highlighting the need to improve the long-time osteointegration and stability of the implants. Another significant drawback of orthopedic implants is stress shielding, which is produced by a stiffness mismatch between the implant and the surrounding bone [5]. The most common material used for biomedical implants is titanium (Ti) and its alloys because of their high biocompatibility and corrosion resistance. However, their elastic modulus (100–120 GPa) is much higher than the one of cancellous (0.02–6 GPa) and cortical bone (3–30 GPa) [6,7].

* Corresponding author.
E-mail address: rasbai@tecnun.es (R. Asbai-Ghoudan).

https://doi.org/10.1016/j.compbiomed.2023.107381
Received 28 April 2023; Received in revised form 21 July 2023; Accepted 14 August 2023
Available online 14 August 2023

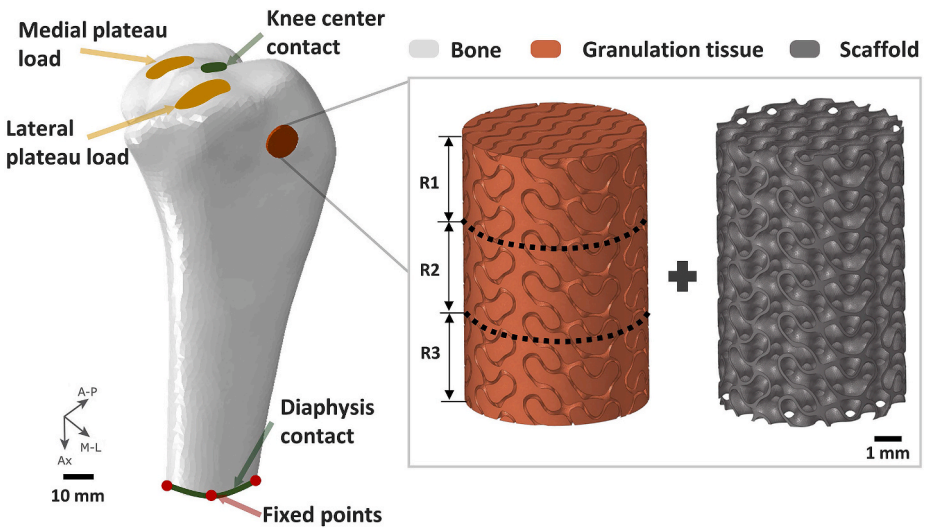

Fig. 1. Model overview with part components and boundary conditions. The knee center contact restricts displacements in the antero-posterior and axial directions and the diaphysis contract restricts axial displacements. The magnitude and distribution of the loads is represented in Table 1. The granulation tissue part shows the periosteal, middle and medullary subregions (R1, R2 and R3 respectively) with the first being the closest to the external surface of the bone.

Table 1
Total applied forces (N) and their directions (axial, antero-posterior and medial-lateral) over the nodes at the medial and lateral plateaus.

Forces on the medial plateau (N)			Forces on the lateral plateau (N)		
Axial	A-P	M-L	Axial	A-P	M-L
−911	−82	−66	−461	−107	13

The structural and material properties of bone undergo constant adaptation and remodeling in response to mechanical loading, resulting in changes in its microarchitecture [8]. Mechanobiology is an emerging field that involves the detailed analysis of how mechanical loads affect bone biology for which engineers and biologists collaborate to unravel this complex interplay [9,10]. Scaffold design and material properties must be optimized to enhance the scaffold's osteointegration and promote bone regeneration [10–12]. Adjusting the apparent stiffness of the scaffold is targeted as it is believed to be one factor that encourages bone ingrowth given the intrinsic relationship between mechanical stimulation and bone adaptation [13]. This requires an exhaustive study of the performance of different scaffold designs.

Additively manufactured (AM) porous metallic biomaterials have been proposed to address the lack of osteointegration in orthopedic implants [14–16]. Amongst their benefits, porous surfaces at the bone-implant interface enhance the biological interaction of the implant with the surrounding bone tissue. The optimization of 3D printed bone scaffolds relies on controlling their mechanical properties to sustain the loads they are subjected to while satisfying the local biomechanical demand [14]. Many works have focused their study on geometrical parameters of lattice bone scaffolds [17–20]. Triply periodic minimal surfaces (TPMS) have shown promising behavior for bone engineering applications in both their skeletal and sheet configurations [21–25]. Besides their outstanding mechanical performance (superior stiffness and better fatigue behavior), their architectural features may have a crucial impact on the diffusion of nutrients and the proliferation and differentiation of cells [26–28]. Also, their versatility allows to easily adapt their porosity and pore size to match a desired stiffness and permeability [29,30].

A few recent works have studied the mechanobiological behavior induced by TMPS geometries. Kelly et al. [31] studied *in vivo* the effect of pore size of gyroid-sheet scaffolds in large femoral defects. In the work of Van hede et al. [32], the authors investigated *in vivo* the optimization of the internal design of intra-oral bone defect scaffolds using a sheet-based gyroid. Jaber et al., 2022 [33] studied and compared both *in silico* and *in vivo* the bone regeneration potential of a strut-based scaffold and a sheet-based gyroid. Although some experimental and numerical works have studied the gyroid architecture in recent years [33–35], none of those works compared the potential to induce mechanobiologially-driven bone regeneration between sheet-based and skeletal-based TPMS architectures. These works showcase the need to further investigate complex porous structures for bone regeneration applications, with all the image-processing and computational difficulties that this entails.

Computational modeling has become a common approach in addressing experimental difficulties and enhancing the comprehension of bone mechanobiology [36–39]. *In silico* modelling allows to use initially calibrated mechanobiological models to run infinite tests in a time and cost-efficient way, enabling the evaluation of potential treatment strategies, thereby diminishing the need for pre-clinical animal experiments [40].

The current *in silico* model for mechanically driven bone regeneration is based on a previous experimental and subject-specific Finite Element (FE) set-up, where the model was fitted with *in vivo* goat data [41]. Small ruminant models are often used in orthopedics research because of the resemblance of their stifle joint to the human knee and compatibilities in bone size and thickness with humans [42–44].The mathematical model of bone mechanoregulation was reduced to a correlation between the bone mineral density and local strain stimulus by considering both the cellular invasion and the mechanical stimulation that lead to bone formation. The bone regeneration potential of different types of complex porous scaffolds was investigated using this model as a predictive tool. The model was then applied to different intra- and post-operative strategies to mimic clinical efforts that aim to boost bone regeneration. A recurrent limitation in scaffold guided bone regeneration is the lack of bone formation in the core of the scaffold [45,46]. The current work analyses the impact of two strategies to overcome this limitation. Firstly, the implantation of a pre-seeded scaffold was studied

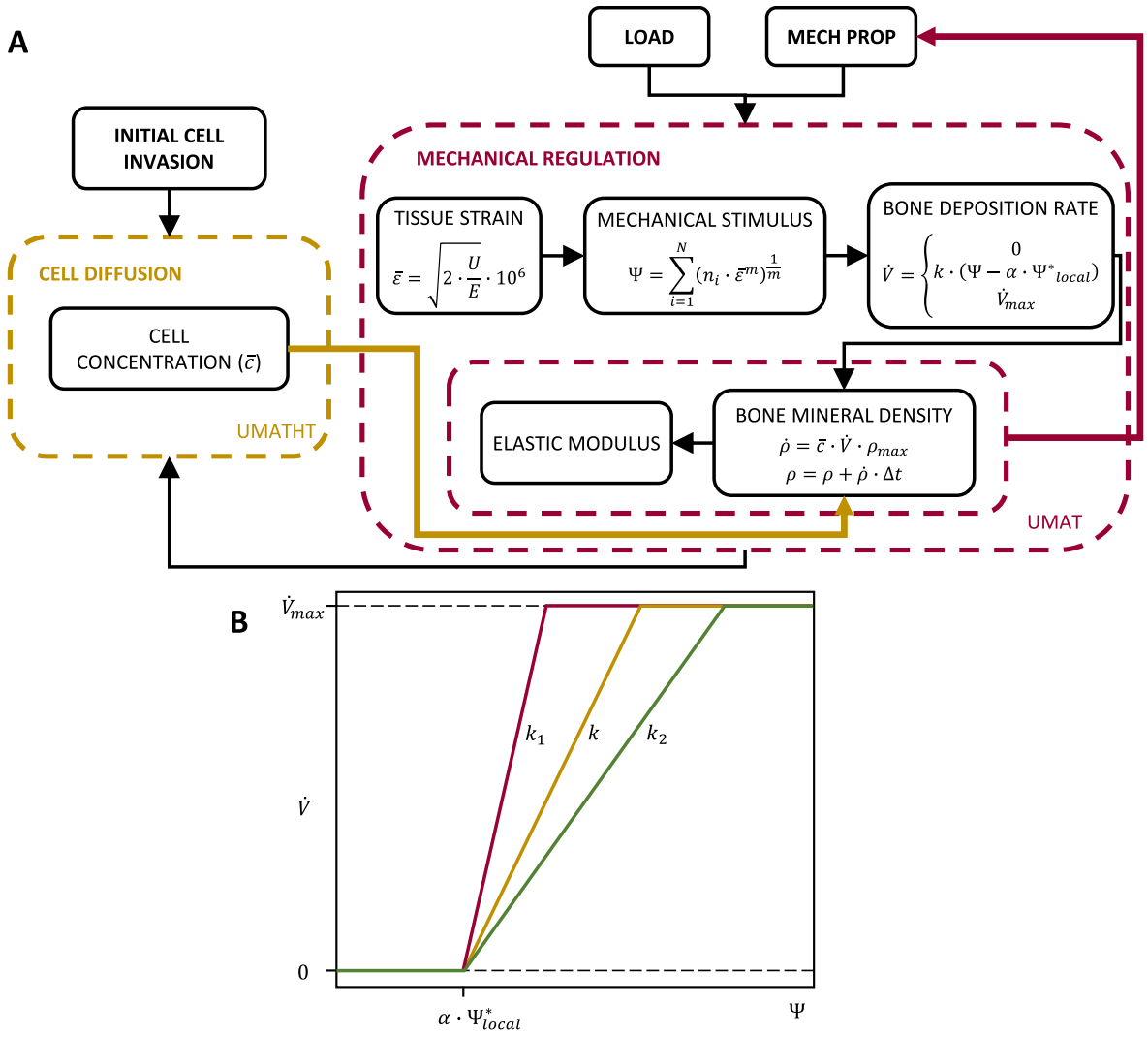

Fig. 2. (A) Overview of the mechanically regulated bone regeneration model with the main mathematical formulation. The model considered a simultaneous process of cell diffusion and bone formation. The mechanical stimulus (Ψ) was obtained from the tissue microstrains and regulated the bone deposition rate ($\dot{V}$). This updated the mechanical properties (density and elastic modulus) of the granulation tissue for the next iteration. Likewise, the cell diffusion updated the cell concentration ($\bar{c}$) for the next iteration. More details on the mechanobiological regulation model can be found in Nasello et al. [41]. (B) Correlation between the bone deposition rate ($\dot{V}$) and the mechanical stimulus (Ψ) representing the mechanosensitivity (k,k_1,k_2) and reduction factor (α). Three mechanosensitivity values were considered where k (yellow) is the model fitted value, k_1 (magenta) is a hypothetical value to represent a higher mechanosensitivity and k_2 (green) is a hypothetical value to represent a lower mechanosensitivity.

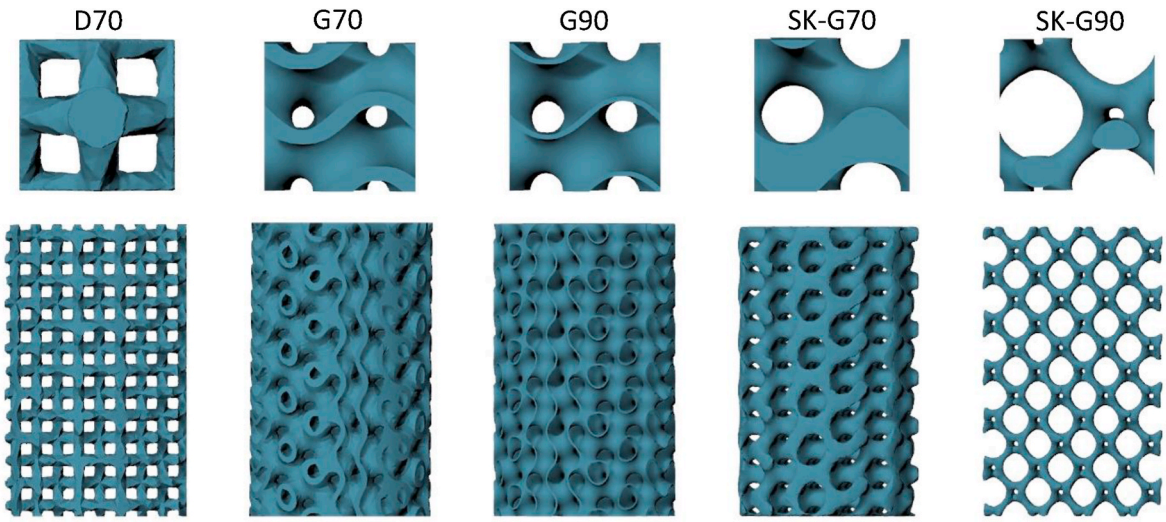

Fig. 3. Unit cell and scaffold representation of the studied designs with their name abbreviations. From left to right: lattice dodecahedron, sheet-based Gyroid 70% and 90% porosities and skeletal-based Gyroid 70% and 90% porosities.

Table 2
Scaffold material properties used in the FE model.

Material	Elastic modulus (MPa)	Poisson ratio	Yield strength (MPa)
Ti	114000	0.3	999[a]
PCL-TCP	400	0.3	12.4[b]

a [65]. b [66].

[47,48]. To improve the performance of acellular scaffolds, strategies such as stem cell therapy, growth factor delivery, or a combination of the two are frequently investigated [47,49]. Huang et al. [50] compared in an *in vivo* rat study the bone regeneration efficiency of a scaffold with and without pre-seeded bone marrow mesenchymal stromal cells and reported that osteogenesis was promoted with a pre-seeded scaffold. Secondly, the effect of increasing the healing period after the surgery was investigated. Li et al. [51] and Henkel et al. [52] studied the effect of extending the post-operative period to three weeks of rest before allowing major loads on the limb, resulting in an increase of the implant osseointegration.

Likewise, certain parameters such as the age or the health of the patient can affect both the mechanical properties of the bone as well as the mechanosensitivity of the subject [53–55]. Nafei et al. [56] studied the relationship between age and the mechanical properties of sheep bones. The work reported that older sheep had values of elastic modulus up to 1.3 times higher than the studied case; while, younger sheep reported values up to 0.5 times lower. The works of Nasello et al. [41] and Sanz-Herrera et al. [57] investigated ranges of values ($1{\cdot}10^{-5}$-$9{\cdot}10^{-4}$ [% $\cdot$ μstrains^{-1} $\cdot$ day^{-1}]) to evaluate and fit the mechanosensitivity of the host on their *in silico* mechanoregulation models. Therefore, changes in the mechanical properties of the bone and the host mechanosensitivity were investigated as well.

The overall aim of this work is to provide a framework to design optimal patient-specific strategies to promote bone regeneration. For this purpose, we have used a goat tibia computational mechano-driven model to, i) investigate the bone regeneration potential of complex porous scaffolds made of two different biocompatible materials; ii) evaluate the impact on the bone regeneration of pre-seeding the implanted scaffold or increasing the post-operative resting period; and iii), assess the influence of patient-specific parameters, such as age and mechanosensitivity. To the best of the authors knowledge, it is the first time such a comprehensive comparison of the bone regeneration potential of complex scaffolds is carried out taking into account architecture, material and clinical strategies for patient-specific applications.

2. Materials and methods

2.1. Mechanobiological regulation model

A previously developed *in silico* mechanoregulation model calibrated with *in vivo* animal data (goat) was adapted to assess the bone regeneration potential of complex porous structures [41]. The study was performed in ABAQUS 2020 (Dassault Systèmes, France) with a linear stress analysis and using user subroutines (UMAT and UMATHT). The tibia was trimmed 10 cm from the proximal region. The trimmed diaphysis had a restricted displacement in the axial direction and 4 nodes along its circumference were tied in all directions. The knee center was tied in the axial and the antero-posterior directions to simulate the ligament insertion [58] (Fig. 1). The study considered a 3.7 year old goat with a weight of 65 kg and the applied loads were scaled from the animal body weight and distributed over the tibial lateral and medial plateaus [59,60] (Fig. 1) (Table 1). More details of the boundary conditions can be found in Fig. A and B of the Supplementary Material. The material properties of the tibia were inferred from CT images [61]. These properties were determined by transforming the Hounsfield Units (HU) from the CT into apparent density and establishing a correlation between the apparent density and the Young's modulus based on existing literature on ovine bone [13].

In this model, a porous scaffold was inserted in the epiphyseal area of a goat tibia and the volume inside of the scaffold's pores was considered as granulation tissue. All the interacting surfaces between the tibia, scaffold and granulation part were modeled with a tie constraint. A diffusion process was considered to model the cell migration from the tibia to the granulation tissue. Cell concentration ($\bar{c}$) was normalized and considered to be 1 at the outer region of the granulation part (tibia-granulation interface) and zero in the scaffold pores.

The model simulated experiments taking place over a 12-week duration. The simulation considered a simultaneous process of cell migration and bone formation. The mechano-regulation algorithm predicted the tissue differentiation taking place in the scaffold pores (granulation tissue) and updated the values of cell concentration and tissue density iteratively. The daily mechanical stimulus (Ψ) was obtained from the effective tissue microstrains ($\bar{\varepsilon}$) during the daily load cycles ($n = 10000$), where m is a model parameter ($m = 4$) and regulated the bone deposition rate ($\dot{V}$) (Fig. 2-A) [41]. The model accounted for

Table 3
Elastic modulus thresholds for histological tissue differentiation [67].

Tissue type E (MPa)	Granulation tissue	Cartilage	Fibrous tissue	Bone
	0.2	2	10	1000

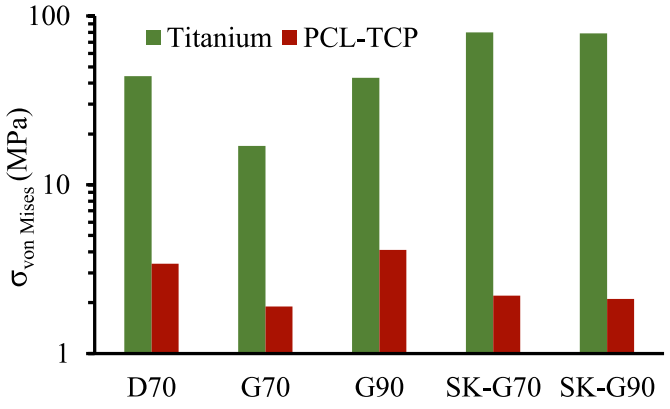

Fig. 4. Maximum value of the von Mises stress distribution for all the analyzed scaffold designs for both materials. From left to right: lattice dodecahedron, sheet-based Gyroid 70% and 90% porosities and skeletal-based Gyroid 70% and 90% porosities.

two variable parameters representing (1) the mechanosensitivity (k) that affects the bone deposition rate ($\dot{V}$) and (2) a reduction factor (α) for the mechanical stimulus that varied based on the implantation site (Fig. 2-B). The considered k parameter was $1{\cdot}10^{-4}$ [% · μstrains^{-1} · day^{-1}] [57,62]; and the reduction factor was set at 50% as fitted in our previous work [41]. The material properties of the newly formed tissue and the normalized cell concentration ($\bar{c}$) in the granulation tissue were updated after each iteration with a UMAT and UMATHT subroutines respectively. The initial density of the granulation tissue was set to 0.001 g/cm^3 and the Poisson's ratio to 0.3. The elastic modulus followed the same continuous correlation between apparent density and Young's modulus used for the tibia; and the density of the granulation tissue was updated based on Eq. (1) and Eq. (2) where ρ_{max} was set to 1.6 g/cm^3 [13]. More details on the mechanobiological regulation model can be found in Nasello et al. [41].

$$\dot{\rho} = \bar{c}\cdot\dot{V}\cdot\rho_{max} \tag{1}$$

$$\rho = \rho + \dot{\rho}\cdot\Delta t \tag{2}$$

2.2. Scaffold and granulation domain design

Five different cylindrical scaffolds were analyzed in this work. The previously experimentally tested scaffold (dodecahedron unit cell) [41] was compared to a Gyroid TPMS geometry in both a sheet and skeletal-based configuration (Eq. (3)), where t is a constant defining the overall geometry of the porous material. The geometries were generated in Rhinoceros 6 (Robert McNeel & Associates, USA) with the use of an in-house code in Grasshopper plug-in. Two porosities (70% and 90%) were considered for each configuration. For the sheet-based scaffolds the t parameter was set to 0 and the obtained mesh was thickened for the 70% and 90% porosities; whereas for the skeletal based configuration the t parameter was modified to generate the 70% and 90% porosity configurations. Each scaffold was referred to according to its architecture and porosity. All the abbreviated names can be found in Fig. 3. The unit cell dimension was 1.9 mm and the structures were 8 mm in diameter and 12 mm in height.

$$cos(x)\cdot sin(y) + cos(y)\cdot sin(z) + cos(z)\cdot sin(x) = t \tag{3}$$

The granulation domain was built by filling the void of the pores of each scaffold. Both parts were then meshed in Hypermesh 2021 (Altair, USA). TPMS geometries have a complex architecture and possess curved surfaces that need a fine mesh to be accurately characterized, which considerably increases the computational cost. A mesh sensitivity analysis was carried out and an element size of 0.15 mm was selected (Supplementary material – Fig. C). The element type used for the simulation were first order tetrahedral elements (C3D4) for the tibia and scaffold parts and hybrid displacement-temperature first order tetrahedral elements (C3D4T) for the granulation part.

The performance of these scaffolds will be studied for two different biocompatible materials with different stiffnesses (Table 2). The stiffer material was titanium (Ti) and to overcome mechanical shielding due to the high stiffness of the scaffold, a less rigid material was studied. Medical-grade polycaprolactone and tricalcium phosphate (PCL-TCP) was considered due to its wide use for biomedical applications [63,64].

The stress distribution of the scaffolds was studied to ensure that both materials provided enough structural integrity and no structure surpassed the material's elastic limit [65,66]. Also, a histology like figure predicting the types of differentiated tissue was obtained based on their elastic modulus. The different thresholds were adjusted based on the values found in the work of Kelly and Prendergast [67] (Table 3).

2.3. Influence of intra- and post-operative strategies

The implantation of a pre-seeded scaffold and the effect of a longer post-operative resting period were studied to observe if the bone formation at the core of the scaffold could be enhanced. For the pre-seeded scaffold, in addition to the already considered cell invasion, a diffusion process from the scaffold's surface to the granulation tissue was modeled with a normalized cell concentration of 1 at the surface. For post-operative resting period, three weeks before allowing major loads on the limb were examined based on other experimental findings [51,52]. The effect of the pre-seeded scaffold and the three-week resting period were analyzed only in one of the models (D70) but both materials (Ti and PCL-TCP) we considered.

Table 4
Bone ingrowth results for the titanium and PCL-TCP scaffolds.

Scaffold	Titanium			PCL-TCP		
	New bone volume (mm^3)	BV/TV (%)	BV/(TV-SV) (%)	New bone volume (mm^3)	BV/TV (%)	BV/(TV-SV) (%)
D70	25.1	5.4	7.0	178.5	38.1	49.9
G70	9.7	2.2	3.2	134.9	30.2	45.1
G90	14.6	3.2	3.6	193.2	42.7	47.7
SK-G70	19.7	4.3	6.3	222.5	49.0	70.9
SK-G90	56.4	12.6	13.7	316.3	70.6	77.0

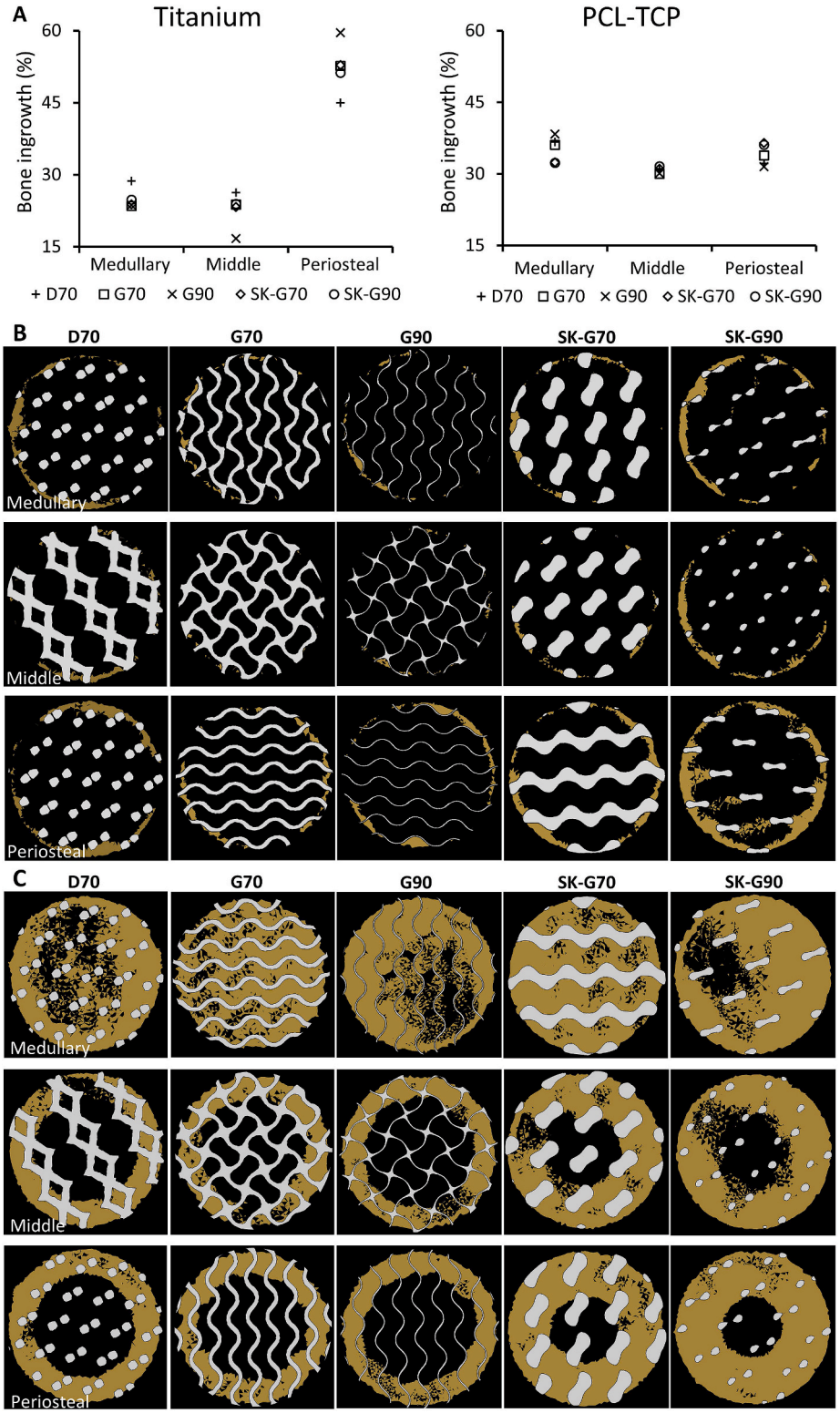

Fig. 5. (A) Predicted bone ingrowth distribution in the medullary, middle and periosteal regions of the scaffold. The values are a percentage of the total bone ingrowth in each scaffold. (B) Representative slices of the bone ingrowth (brown) in the medullary, middle and periosteal regions at a height of 1 mm, 5.5 mm and 9 mm respectively for each one of the titanium scaffolds. (C) Representative slices of the bone ingrowth (brown) in the medullary, middle and periosteal regions at a height of 1 mm, 5.5 mm and 9 mm respectively for each one of the PCL-TCP scaffolds.

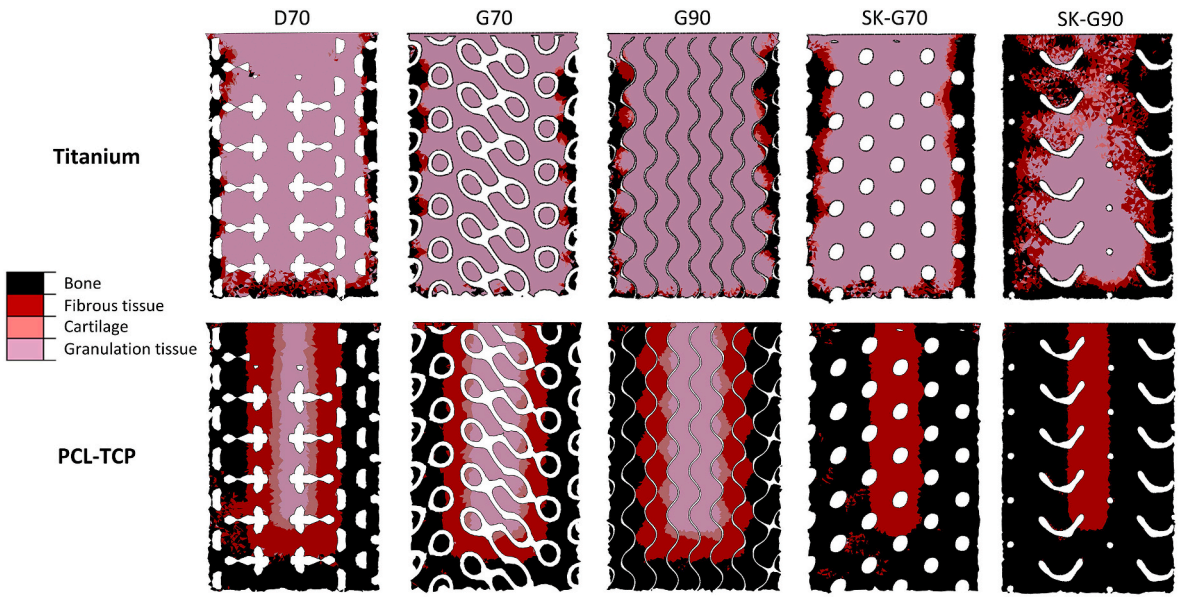

Fig. 6. Middle slice with the histology predictions after 12 weeks for the titanium and PCL-TCP scaffolds.

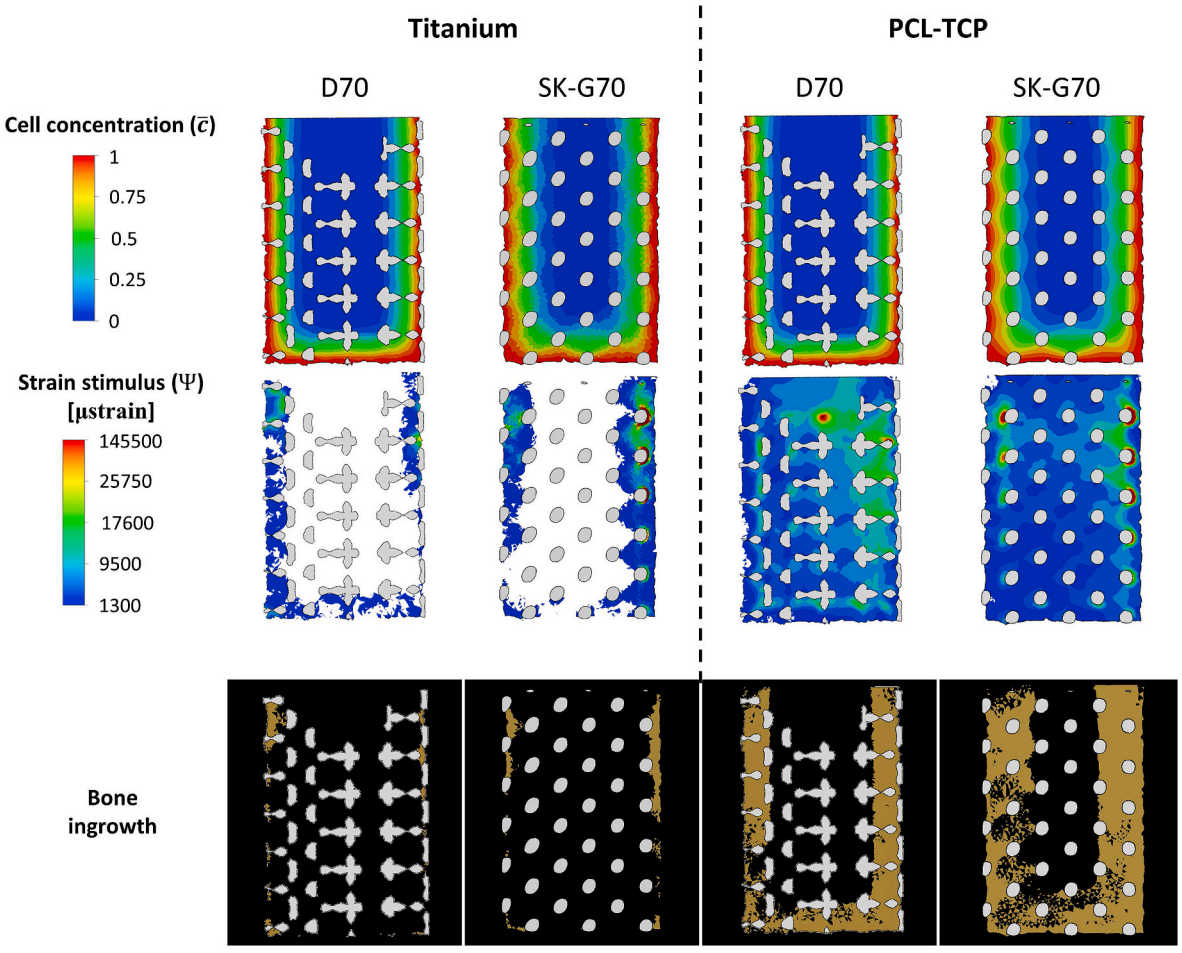

Fig. 7. Middle slices representing the cell concentration, the areas with a strain stimulus higher than the reference stimulus ($\alpha \cdot \Psi^{s}_{local}$) and the bone ingrowth after 12 weeks of the D70 and SK-G70 scaffolds for the titanium models and the PCL-TCP models.

Table 5
Observed bone ingrowth for the non-seeded, seeded and 3-week post-operative rest cases for both titanium and PCL-TCP scaffold materials.

Scaffold	Titanium			PCL-TCP		
	New bone volume (mm^3)	BV/TV (%)	BV/(TV-SV) (%)	New bone volume (mm^3)	BV/TV (%)	BV/(TV-SV) (%)
Baseline (D70)	25.1	5.4	7.0	178.5	38.1	49.9
Seeded	27.6	5.9	7.7	271.4	57.9	75.8
3-week rest	31.1	6.6	8.7	229.8	49.0	64.2

2.4. Aging and mechanosensitivity

To assess the influence of patient-specific parameters, four hypothetical cases were compared by scaling the bone mechanical properties by factors of 1.25 and 0.75, following the findings of Nafei et al. [56] and by modifying the subject's mechanoregulation factor of bone deposition rate (k_1, k_2), according to the values investigated in the literature [41, 57] (Fig. 2-B). The case studies considered (1) an elderly subject with stiffer bones by scaling the bone material properties by 1.25, (2) the same elderly subject with a lower mechanoregulation factor ($k_2 = 5{\cdot}10^{-5}$ [$\% \cdot \mu strains^{-1} \cdot day^{-1}$]), (3) a younger subject with more flexible bones by scaling the bone mechanical properties by 0.75 and (4) the same younger subject with a higher mechanoregulation factor ($k_1 = 2{\cdot}10^{-4}$ [$\% \cdot \mu strains^{-1} \cdot day^{-1}$]). These changes were only studied in one of the models (D70) and the study with the fitted parameters will be considered as the baseline case to perform the comparison. All the differences will be expressed in relative percentages.

2.5. Bone ingrowth quantification

A 0.25 g/cm^3 was considered to be the density threshold to consider the newly formed tissue as trabecular bone [13]. The condition for the tissue density changes at each element of the granulation tissue was dependent on the cell concentration and the strain stimulus at said element. The normalized cell concentration was analyzed in the range of 0–1 to observe the effect of the scaffold geometry on the cellular diffusion process. The evolution of the strain stimulus was observed as the bone density and elastic modulus of the newly formed bone were updated throughout the simulation period. The bone ingrowth volume was obtained by adding up the element volume of all the mesh elements with a density above the threshold to be considered bone (0.25 g/cm^3). To calculate the relative bone ingrowth, the volume of newly formed bone into the scaffolds (BV) was measured and divided by the total defect volume (TV) minus the scaffold volume (SV) in the *in silico* model. The total volume percentage was also obtained as BV/TV analogous to the measure used clinically. Three different subregions of the scaffolds were discretized to perform a more refined bone quantification. The medullary, middle and periosteal subregions were 3.7 mm each with the latter being the closest to the external surface of the bone (R1-3 in Fig. 1).

3. Results

3.1. Scaffold regeneration potential

The von Mises stress distribution of all of the scaffolds showed that both materials provided enough structural integrity. The yield strength (σ_y) (Table 2) was not reached in any of the studied scaffolds (Fig. 4). G70 resulted to have the lowest stress concentration for both of the materials, while SK-G70 and G90 had the highest values for the titanium and PCL-TCP respectively.

The bone ingrowth induced by the studied scaffolds is shown in Table 4. For the titanium scaffold, the highest bone ingrowth was seen for SK-G90 at 13.7% followed by D70, SK-G70, G90 and G70 at 7.0%, 6.3%, 3.6% and 2.2% respectively. When considering PCL-TCP as the scaffold material, the highest bone ingrowth was seen for the SK-G90 with 77%. SK-G70, D70, G90 and G70, arranged in a decreasing order, reported values of bone ingrowth between 70.9% and 45.1%.

A different result was observed in each structure based on the studied subregion. Fig. 5-A shows the percentage of the total bone ingrowth that took place in the medullary, middle and periosteal regions. For the titanium scaffolds, D70 seemed to have the highest relative bone ingrowth in the medullary and middle regions with regard to the total volume of bone predicted for each scaffold. Likewise, G90 had the best relative performance in the periosteal region. G70, SK-G70 and SK-G90 exhibited a similar behavior in all three subregions. The results for the softer material showed a more even distribution of the proportion of regenerated bone over the medullary, middle and periosteal regions (30–40% in each). Fig. 5-B and 5-C present slices from each area representing how the bone regenerated in each model. On the histology like representation of the predicted tissue differentiation (Fig. 6), it can be observed that the results for the titanium scaffolds primarily showed the presence of granulation tissue due to the scaffold's high stiffness, whereas the soft material scaffolds predicted a higher volume of bone and fibrous tissue to be differentiated.

This analysis also reported that D70 had a larger bone ingrowth than SK-G70 for the titanium scaffolds but the outcome was inversed when studying the PCL-TCP material (Table 4). It was observed that the geometrical features of the SK-G70 allowed for a better cell diffusion but the titanium material restricted the bone regeneration due to a more localized stimulus. However, when the softer material was used, the mechanical stimulus reached more central areas and the cell diffusion advantage was translated in a higher bone ingrowth (Fig. 7).

3.2. Pre-seeded scaffold and healing period

The results of inserting a titanium pre-seeded scaffold showed that although the total bone ingrowth increased in a 10% with respect to the non-seeded case (Table 5), all of the new bone was located in the outer region of the scaffold. For the PCL-TCP scaffolds, the bone ingrowth reached the inner pores of the scaffold and the bone ingrowth had a remarkable increase from 49.9% to 75.8% (Fig. 8).

The influence of the three-week post-operative resting period studied for the titanium models showed that bone ingrowth took place mainly in the external pores of the scaffold, with a limited ingrowth the core region. The percentage of bone ingrowth increased with regard to considering only one day resting (8.7% vs 7.0%) (Table 5). Moreover, when considering the less stiff material, the bone reached a more central part of the scaffold but did not reach the core (Fig. 8). However, the bone volume increased considerably.

3.3. Influence of age and mechanosensitivity

The study to assess the influence of patient-specific parameters showed that when the bone's initial elastic modulus is higher (case 1), the resultant bone ingrowth was 6.8% lower than the fitted model (baseline case) (Fig. 9). The same phenomenon could be observed when, aside from raising the elastic modulus, the mechanosensitivity

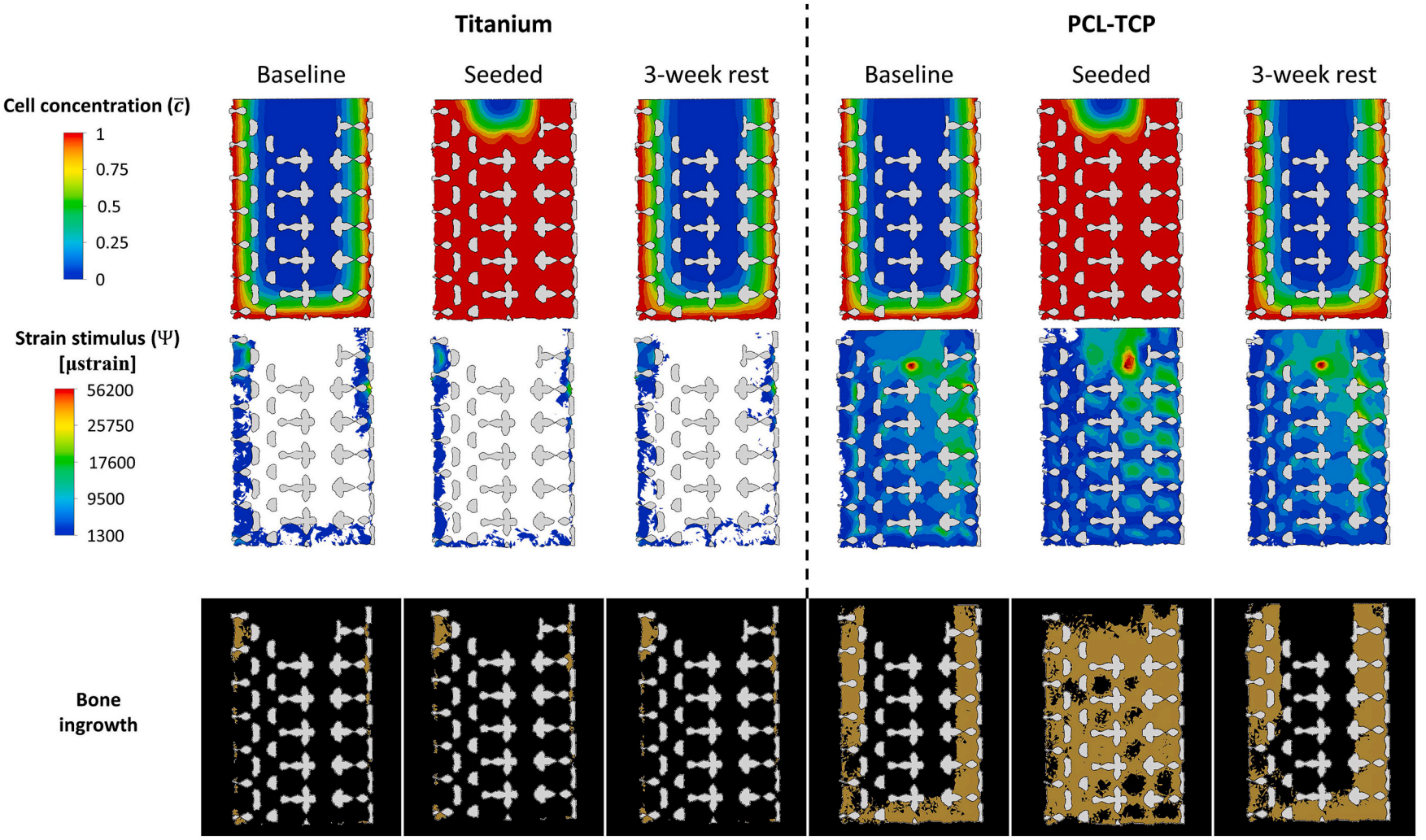

Fig. 8. Middle slices representing the cell concentration, the areas with a strain stimulus higher than the reference stimulus ($\alpha \cdot \Psi^{*}_{local}$) and the bone ingrowth after 12 weeks for the baseline, the pre-seeded scaffold and the 3-week post-operative rest studies for both Ti (left) and PCL-TCP materials (right).

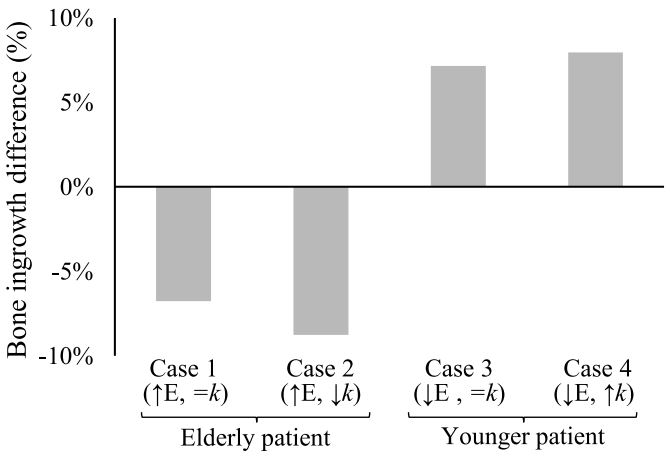

Fig. 9. Influence of patient-specific parameters in the bone ingrowth predictions with respect to the fitted model (baseline case).

parameter was lowered, as the results for case 2 showed an 8.8% decrease of the predicted bone ingrowth. However, this tendency was inverted when a lower bone's elastic modulus was studied as case 3 resulted in a 7.2% increase compared to the baseline case. Likewise, when aside of lowering the elastic modulus, the mechanosensitivity parameter was raised, the predicted bone ingrowth volume reported an 8.0% increase.

4. Discussion

This work successfully quantified the mechanobiological potential of complex porous scaffolds and compared the influence of their geometrical properties when considering different stiffness materials.

Five different scaffolds were designed to characterize their bone regeneration capability. The skeletal gyroid scaffold with 90% porosity (SK-G90) consistently showed the highest bone formation in both material analyses. When comparing the performance of each scaffold, it was observed that the cell diffusion was influenced by the geometrical features, but the presence of cells was only translated in bone ingrowth when mechanical stimulus was in the desired range (Fig. 7). A considerable difference in the resulting bone ingrowth for both studied materials was also observed. The increase in the relative bone ingrowth ranged from fourteen times (G90) to five times (SK-G90) when comparing PCL-TCP with Ti. This shows that the scaffold design is as important as the material when studying their mechanobiological potential.

To induce bone formation, the osteocyte concentration should be high enough in the scaffold surroundings and the mechanical stimulation needs to be in the range for bone formation. Titanium was observed to be too stiff for this application as mechanical shielding limited the bone tissue formation. This work studied the performance of a softer scaffold to bypass this phenomenon and the results were satisfactory. When considering PCL-TCP the bone ingrowth increased in all the studied cases. In agreement with these results, other works of the literature also reported that softer scaffold material composites have a great osteoregenerative potential as they can match the elastic modulus of cancellous bone [64,68,69]. Topological optimization was also investigated by other works to overcome the shielding limitation [15,70].

It is important to note that this work shows that the skeletal-based scaffolds show a higher bone regeneration behavior than the sheet-based, contrary to what could be inferred from only observing their mechanical behavior [34]. One possible explanation is the different diffusion properties of each configuration as the skeletal models reported higher cell concentrations in more central regions of the scaffolds (Fig. 10). This highlights the need of more complex models, such as computational mechanobiology models, that combine different relevant variables to accurately characterize bone scaffolds.

The geometrical properties of the scaffolds play an important role in bone formation as the distribution of the newly formed bone was different based on the regions of the scaffold. Parameters such as the pore size or shape influence the strain distribution and thus, control the mechanical stimulation to induce bone differentiation. According to the subregion of interest (medullary, middle and periosteal), each scaffold showed a different volume of newly formed bone. All these variables, in addition to the location of the scaffold and the direction of the applied loads suggest that there is no universal scaffold design that would be optimal for all applications; instead, the information obtained from these analyses could be used to optimize the implant design to target localized bone formation.

In some cases, it was observed that no bone formation took place in the core of the scaffold because of a low cell concentration as the cells did not reach the inner pores (Fig. 7). The use of a pre-seeded scaffold was examined to allow cells to increase their concentration at the inner pores, as suggested in the literature [50]. This improved the bone ingrowth for the titanium scaffold but mechanical shielding avoided bone formation in the core region (Fig. 8). However, when considering a pre-seeded scaffold with a softer material, the predicted newly formed bone clearly reached the central part of the scaffold (Fig. 8). Another investigated approach to improve the cell concentration is extending the recovery time before applying any stress on the affected limb [51,52]. This allows cells to migrate and proliferate and reach the center of the scaffold so when the area is mechanically stimulated, either by walking or by physiotherapy, bone ingrowth can be more effective.

Age and metabolic diseases such as osteoporosis or osteopetrosis are issues that can affect the bone structure and its mechanical properties. In those cases, the reduction in mechanical properties is accompanied by a change in the normal metabolic balance and affect the bone formation rate [71,72]. These changes were studied; and although the used parameters only varied slightly as they were hypothetical, the bone

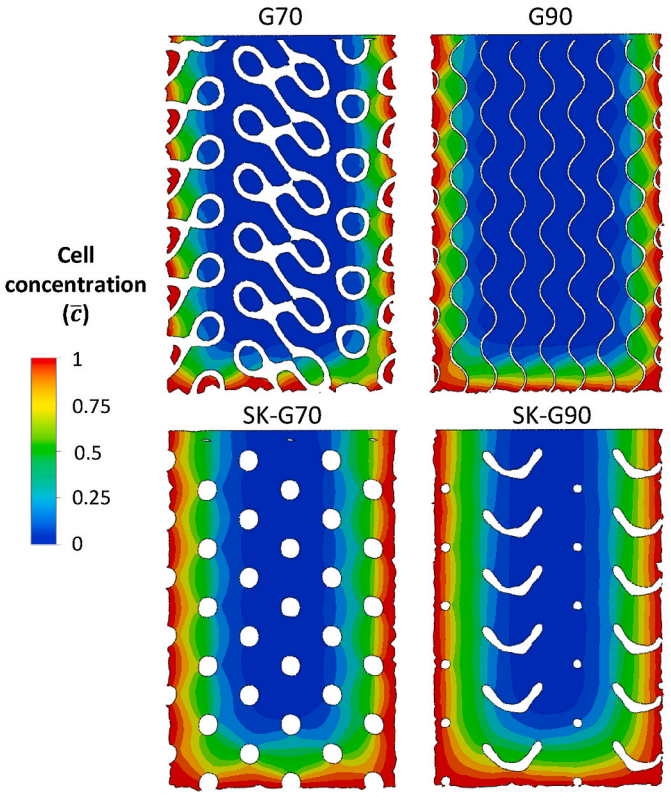

Fig. 10. Cell concentration diagram comparing the diffusion in the G70, G90, SK-G70 and SK-G90 scaffolds.

regeneration process showed different outcomes. The variation in the patient-specific parameters reported differences of up to 16% in the estimated bone regeneration. This fact highlights the significance of accurately reproducing such parameters in the analysis in order to use computational models as a presurgical tool to assess what type of scaffold would be more suitable for each application.

There are some limitations and assumptions in this study that could be improved. The mechanoregulation model only accounts for bone deposition within the granulation area, ignoring the bone remodeling process and its potential consequences. However, due to the scaffolds' non-load bearing capacity, it was assumed that this phenomenon would not cause significant variations in the results. In addition, cell diffusion and proliferation were modeled as a simple diffusion process that only considered the tissue density and a diffusion constant. Oxygen concentration, nutrient diffusion and angiogenesis are parameters that can help represent more accurately the cell proliferation and osteogenic differentiation [73,74]. Nonetheless, these modifications are not expected to greatly alter the comparison between the scaffolds' bone regeneration potential.

Making use of advanced manufacturing techniques, future lines of work could investigate novel scaffold designs to optimize cell diffusion while also enhancing the stress distributions. The soft material studied in this work is ideal because the scaffolds are not weight bearing. For weight bearing applications, these scaffolds might need an additional support or the study and design of new metamaterials that could provide enough structural integrity whilst maintaining the mechanical stimulus in the desired range of bone differentiation.

5. Conclusions

This work successfully studied complex scaffold designs using a computational mechanobiology model as a tool to investigate their bone regeneration potential. The scaffold's mechanical interaction with the subject is determined by factors such as the local environment and the response of the host; affecting greatly the volume and distribution of bone that is formed within the scaffold. The impact of the scaffold's geometry and material were investigated and proved to affect bone regeneration. The scaffold's geometrical properties showed different diffusion patterns that affected the regenerated bone volume. The ability to induce mechanobiologically-driven bone regeneration of the scaffolds was also seen to be dependent on the material, suggesting that the material can be used to tune the strain distribution and enhance the bone ingrowth. Likewise, physiological characteristics of the host need to be assessed as variations in the bone mineral density or the mechanosensitivity of the subject can influence the suitability of one scaffold design or another.

Declaration of competing interest

The authors declare that they have no known competing financial interests or personal relationships that could have appeared to influence the work reported in this paper.

Acknowledgements

RAG is grateful for the financial support for an international mobility by Programa de ayudas de movilidad de la Fundación Bancaria La Caixa. SRG and NRF are grateful for the support by Proyecto de Generación de Conocimiento (PID2021-126471OA-I00). MAP is grateful for the support by the Spanish Ministry of Science and Innovation Grant No PID2020-113819RB-I00.

Appendix A. Supplementary data

Supplementary data to this article can be found online at https://doi.org/10.1016/j.compbiomed.2023.107381.

References

[1] Z. Wang, et al., Pharmaceutical electrospinning and 3D printing scaffold design for bone regeneration, Adv. Drug Deliv. Rev. 174 (2021) 504–534, https://doi.org/10.1016/j.addr.2021.05.007. Jul.
[2] S. Yin, W. Zhang, Z. Zhang, X. Jiang, Recent advances in scaffold design and material for vascularized tissue-engineered bone regeneration, Adv. Healthcare Mater. 8 (10) (2019), 1801433, https://doi.org/10.1002/adhm.201801433.
[3] S. Kurtz, K. Ong, E. Lau, F. Mowat, M. Halpern, Projections of primary and revision hip and knee arthroplasty in the United States from 2005 to 2030, J Bone Joint Surg Am 89 (4) (Apr. 2007) 780–785, https://doi.org/10.2106/JBJS.F.00222.
[4] S.D. Ulrich, et al., Total hip arthroplasties: what are the reasons for revision? Inter. Orthopaedics 32 (5) (Oct. 2008) 597–604, https://doi.org/10.1007/s00264-007-0364-3.
[5] A. Palmquist, M. Jolic, E. Hryha, F.A. Shah, Complex geometry and integrated macro-porosity: clinical applications of electron beam melting to fabricate bespoke bone-anchored implants, Acta Biomater. 156 (Jan. 2023) 125–145, https://doi.org/10.1016/j.actbio.2022.06.002.
[6] D. Martinez-Marquez, Y. Delmar, S. Sun, R.A. Stewart, Exploring macroporosity of additively manufactured titanium metamaterials for bone regeneration with quality by design: a systematic literature review, Materials 13 (21) (Jan. 2020) 21, https://doi.org/10.3390/ma13214794.
[7] S. Safavi, Y. Yu, D.L. Robinson, H.A. Gray, D.C. Ackland, P.V.S. Lee, Additively manufactured controlled porous orthopedic joint replacement designs to reduce bone stress shielding: a systematic review, J. Orthop. Surg. Res. 18 (1) (2023) 42, https://doi.org/10.1186/s13018-022-03492-9. Jan.
[8] J.M. García-Aznar, G. Nasello, S. Hervas-Raluy, M.Á. Pérez, M.J. Gómez-Benito, Multiscale modeling of bone tissue mechanobiology, Bone 151 (Oct. 2021), 116032, https://doi.org/10.1016/j.bone.2021.116032.
[9] S.W. Verbruggen, L.M. McNamara, Chapter 6 - bone mechanobiology in health and disease, in: S.W. Verbruggen (Ed.), Mechanobiology in Health and Disease, Academic Press, 2018, pp. 157–214, https://doi.org/10.1016/B978-0-12-812952-4.00006-4.
[10] A.-M. Pobloth, et al., Mechanobiologically optimized 3D titanium-mesh scaffolds enhance bone regeneration in critical segmental defects in sheep, Sci. Transl. Med. 10 (423) (Jan. 2018) eaam8828, https://doi.org/10.1126/scitranslmed.aam8828.
[11] J.M. Shum, et al., Enhanced bone formation in locally-optimised, low-stiffness additive manufactured titanium implants: an in silico and in vivo tibial advancement study, Acta Biomater. 156 (Jan. 2023) 202–213, https://doi.org/10.1016/j.actbio.2022.04.006.
[12] J. Wieding, T. Lindner, P. Bergschmidt, R. Bader, Biomechanical stability of novel mechanically adapted open-porous titanium scaffolds in metatarsal bone defects of sheep, Biomaterials 46 (Apr. 2015) 35–47, https://doi.org/10.1016/j.biomaterials.2014.12.010.
[13] S. Ghouse, et al., The design and in vivo testing of a locally stiffness-matched porous scaffold, Appl. Mater. Today 15 (Jun. 2019) 377–388, https://doi.org/10.1016/j.apmt.2019.02.017.
[14] A.A. Zadpoor, Additively manufactured porous metallic biomaterials, J. Mater. Chem. B 7 (26) (Jul. 2019) 4088–4117, https://doi.org/10.1039/C9TB00420C.
[15] M. Alaña, A. Lopez-Arancibia, S. Ghouse, N. Rodriguez-Florez, S. Ruiz de Galarreta, Additively manufactured lattice structures with controlled transverse isotropy for orthopedic porous implants, Comput. Biol. Med. 150 (Nov. 2022), 105761, https://doi.org/10.1016/j.compbiomed.2022.105761.
[16] H. Chen, et al., Design and properties of biomimetic irregular scaffolds for bone tissue engineering, Comput. Biol. Med. 130 (Mar. 2021), 104241, https://doi.org/10.1016/j.compbiomed.2021.104241.
[17] V.J. Challis, A.P. Roberts, J.F. Grotowski, L.-C. Zhang, T.B. Sercombe, Prototypes for bone implant scaffolds designed via topology optimization and manufactured by solid freeform fabrication, Adv. Eng. Mater. 12 (11) (2010) 1106–1110, https://doi.org/10.1002/adem.201000154.
[18] Y. Zheng, Q. Han, J. Wang, D. Li, Z. Song, J. Yu, Promotion of osseointegration between implant and bone interface by titanium alloy porous scaffolds prepared by 3D printing, ACS Biomater. Sci. Eng. 6 (9) (Sep. 2020) 5181–5190, https://doi.org/10.1021/acsbiomaterials.0c00662.
[19] N. Abbasi, S. Hamlet, R.M. Love, N.-T. Nguyen, Porous scaffolds for bone regeneration, J. Sci.: Advan. Mater. Devices 5 (1) (Mar. 2020) 1–9, https://doi.org/10.1016/j.jsamd.2020.01.007.
[20] J.C. Reichert, et al., Custom-made composite scaffolds for segmental defect repair in long bones, Int. Orthop. 35 (8) (Aug. 2011) 1229–1236, https://doi.org/10.1007/s00264-010-1146-x.
[21] S. Ma, K. Song, J. Lan, L. Ma, Biological and mechanical property analysis for designed heterogeneous porous scaffolds based on the refined TPMS, J. Mech. Behav. Biomed. Mater. 107 (2020), 103727, https://doi.org/10.1016/j.jmbbm.2020.103727. Jul.
[22] D. Ali, M. Ozalp, S.B.G. Blanquer, S. Onel, Permeability and fluid flow-induced wall shear stress in bone scaffolds with TPMS and lattice architectures: a CFD analysis, Eur. J. Mech. B Fluid 79 (Jan. 2020) 376–385, https://doi.org/10.1016/j.euromechflu.2019.09.015.
[23] A.P.G. Castro, R.B. Ruben, S.B. Gonçalves, J. Pinheiro, J.M. Guedes, P. R. Fernandes, Numerical and experimental evaluation of TPMS Gyroid scaffolds for bone tissue engineering, Comput. Methods Biomech. Biomed. Eng. 22 (6) (2019) 567–573, https://doi.org/10.1080/10255842.2019.1569638. Apr.
[24] O. Al-Ketan, D.-W. Lee, R. Rowshan, R.K. Abu Al-Rub, Functionally graded and multi-morphology sheet TPMS lattices: design, manufacturing, and mechanical properties, J. Mech. Behav. Biomed. Mater. 102 (Feb. 2020), 103520, https://doi.org/10.1016/j.jmbbm.2019.103520.

[25] H. Montazerian, et al., Permeability and mechanical properties of gradient porous PDMS scaffolds fabricated by 3D-printed sacrificial templates designed with minimal surfaces, Acta Biomater. 96 (Sep. 2019) 149–160, https://doi.org/10.1016/j.actbio.2019.06.040.
[26] T. Poltue, C. Karuna, S. Khrueaduangkham, S. Seehanam, P. Promoppatum, Design exploration of 3D-printed triply periodic minimal surface scaffolds for bone implants, Int. J. Mech. Sci. 211 (2021), 106762, https://doi.org/10.1016/j.ijmecsci.2021.106762. Dec.
[27] L. Zhang, et al., Energy absorption characteristics of metallic triply periodic minimal surface sheet structures under compressive loading, Addit. Manuf. 23 (Oct. 2018) 505–515, https://doi.org/10.1016/j.addma.2018.08.007.
[28] D. Ali, Effect of scaffold architecture on cell seeding efficiency: a discrete phase model CFD analysis, Comput. Biol. Med. 109 (Jun. 2019) 62–69, https://doi.org/10.1016/j.compbiomed.2019.04.025.
[29] O. Al-Ketan, R.K. Abu Al-Rub, R. Rowshan, The effect of architecture on the mechanical properties of cellular structures based on the IWP minimal surface, J. Mater. Res. 33 (3) (2018) 343–359, https://doi.org/10.1557/jmr.2018.1. Feb.
[30] R. Asbai-Ghoudan, S. Ruiz de Galarreta, N. Rodriguez-Florez, Analytical model for the prediction of permeability of triply periodic minimal surfaces, J. Mech. Behav. Biomed. Mater. 124 (Dec. 2021), 104804, https://doi.org/10.1016/j.jmbbm.2021.104804.
[31] C.N. Kelly, et al., Functional repair of critically sized femoral defects treated with bioinspired titanium gyroid-sheet scaffolds, J. Mech. Behav. Biomed. Mater. 116 (Apr. 2021), 104380, https://doi.org/10.1016/j.jmbbm.2021.104380.
[32] D. Van hede, et al., 3D-Printed synthetic hydroxyapatite scaffold with in silico optimized macrostructure enhances bone formation in vivo, Adv. Funct. Mater. 32 (6) (2022), 2105002, https://doi.org/10.1002/adfm.202105002.
[33] M. Jaber, P.S.P. Poh, G.N. Duda, S. Checa, PCL strut-like scaffolds appear superior to gyroid in terms of bone regeneration within a long bone large defect: an in silico study, Front. Bioeng. Biotechnol. 10 (2022). Accessed: May 11, 2023. [Online]. Available: https://www.frontiersin.org/articles/10.3389/fbioe.2022.995266.
[34] O. Al-Ketan, R. Rowshan, R.K. Abu Al-Rub, Topology-mechanical property relationship of 3D printed strut, skeletal, and sheet based periodic metallic cellular materials, Addit. Manuf. 19 (Jan. 2018) 167–183, https://doi.org/10.1016/j.addma.2017.12.006.
[35] A. Yánez, A. Cuadrado, O. Martel, H. Afonso, D. Monopoli, Gyroid porous titanium structures: a versatile solution to be used as scaffolds in bone defect reconstruction, Mater. Des. 140 (Feb. 2018) 21–29, https://doi.org/10.1016/j.matdes.2017.11.050.
[36] S.W. Verbruggen, T.J. Vaughan, L.M. McNamara, Strain amplification in bone mechanobiology: a computational investigation of the in vivo mechanics of osteocytes, J. R. Soc. Interface 9 (75) (Oct. 2012) 2735–2744, https://doi.org/10.1098/rsif.2012.0286.
[37] D. Lacroix, P.J. Prendergast, A mechano-regulation model for tissue differentiation during fracture healing: analysis of gap size and loading, J. Biomech. 35 (9) (Sep. 2002) 1163–1171, https://doi.org/10.1016/S0021-9290(02)00086-6.
[38] C. Metz, G.N. Duda, S. Checa, Towards multi-dynamic mechano-biological optimization of 3D-printed scaffolds to foster bone regeneration, Acta Biomater. 101 (Jan. 2020) 117–127, https://doi.org/10.1016/j.actbio.2019.10.029.
[39] Q. Shi, H. Shui, Q. Chen, Z.-Y. Li, How does mechanical stimulus affect the coupling process of the scaffold degradation and bone formation: an in silico approach, Comput. Biol. Med. 117 (Feb. 2020), 103588, https://doi.org/10.1016/j.compbiomed.2019.103588.
[40] M. Viceconti, E. Dall'Ara, From bed to bench: how in silico medicine can help ageing research, Mech. Ageing Dev. 177 (Jan. 2019) 103–108, https://doi.org/10.1016/j.mad.2018.07.001.
[41] G. Nasello, et al., Mechano-driven regeneration predicts response variations in large animal model based on scaffold implantation site and individual mechano-sensitivity, Bone 144 (Mar. 2021), 115769, https://doi.org/10.1016/j.bone.2020.115769.
[42] I.E. Dias, et al., Mesenchymal stem cell studies in the goat model for biomedical research—a review of the scientific literature, Biology 11 (9) (Sep. 2022), https://doi.org/10.3390/biology11091276. Art. no. 9.
[43] C.R. Chu, M. Szczodry, S. Bruno, Animal models for cartilage regeneration and repair, Tissue Eng. B Rev. 16 (1) (Feb. 2010) 105–115, https://doi.org/10.1089/ten.teb.2009.0452.
[44] A. Chevrier, A.S.M. Kouao, G. Picard, M.B. Hurtig, M.D. Buschmann, Interspecies comparison of subchondral bone properties important for cartilage repair, J. Orthop. Res. 33 (1) (2015) 63–70, https://doi.org/10.1002/jor.22740.
[45] S.K. Gummadi, A. Saini, J.S. Owusu-Danquah, P. Sikder, Mechanical properties of 3D-printed porous poly-ether-ether-ketone (PEEK) orthopedic scaffolds, J. Occup. Med. 74 (9) (2022) 3379–3391, https://doi.org/10.1007/s11837-022-05361-6. Sep.
[46] K.S. Rappe, et al., On-growth and in-growth osseointegration enhancement in PM porous Ti-scaffolds by two different bioactivation strategies: alkali thermochemical treatment and RGD peptide coating, Int. J. Mol. Sci. 23 (3) (Jan. 2022), https://doi.org/10.3390/ijms23031750. Art. no. 3.
[47] J.R. Porter, T.T. Ruckh, K.C. Popat, Bone tissue engineering: a review in bone biomimetics and drug delivery strategies, Biotechnol. Prog. 25 (6) (2009) 1539–1560, https://doi.org/10.1002/btpr.246.
[48] H. Xu, et al., Stem cell-seeded 3D-printed scaffolds combined with self-assembling peptides for bone defect repair, Tissue Eng. 28 (3–4) (Feb. 2022) 111–124, https://doi.org/10.1089/ten.tea.2021.0055.
[49] J. Xue, C. Qin, C. Wu, 3D printing of cell-delivery scaffolds for tissue regeneration, Regenerative Biomater. 10 (Jan. 2023) rbad032, https://doi.org/10.1093/rb/rbad032.
[50] Y. Huang, Z. Huang, H. Liu, X. Zhang, Q. Cai, X. Yang, Photoluminescent biodegradable polyorganophosphazene: a promising scaffold material for in vivo application to promote bone regeneration, Bioact. Mater. 5 (1) (Mar. 2020) 102–109, https://doi.org/10.1016/j.bioactmat.2020.01.008.
[51] Z. Li, D. Betts, G. Kuhn, M. Schirmer, R. Müller, D. Ruffoni, Mechanical regulation of bone formation and resorption around implants in a mouse model of osteopenic bone, J. R. Soc. Interface 16 (152) (Mar. 2019), 20180667, https://doi.org/10.1098/rsif.2018.0667.
[52] J. Henkel, et al., Scaffold-guided bone regeneration in large volume tibial segmental defects, Bone 153 (Dec. 2021), 116163, https://doi.org/10.1016/j.bone.2021.116163.
[53] H. Leng, M.J. Reyes, N.X. Dong, X. Wang, Effect of age on mechanical properties of the collagen phase in different orientations of human cortical bone, Bone 55 (2) (Aug. 2013) 288–291, https://doi.org/10.1016/j.bone.2013.04.006.
[54] E.F. Morgan, G.U. Unnikrisnan, A.I. Hussein, Bone mechanical properties in healthy and diseased states, Annu. Rev. Biomed. Eng. 20 (Jun. 2018) 119–143, https://doi.org/10.1146/annurev-bioeng-062117-121139.
[55] D.B. Burr, Changes in bone matrix properties with aging, Bone 120 (Mar. 2019) 85–93, https://doi.org/10.1016/j.bone.2018.10.010.
[56] A. Nafei, C.C. Danielsen, F. Linde, I. Hvid, Properties of growing trabecular ovine bone: part I: mechanical and physical properties, J. Bone Joint Surg. British 82 (6) (Aug. 2000) 910–920, https://doi.org/10.1302/0301-620x.82b6.0820910.
[57] J.A. Sanz-Herrera, J.M. García-Aznar, M. Doblaré, On scaffold designing for bone regeneration: a computational multiscale approach, Acta Biomater. 5 (1) (Jan. 2009) 219–229, https://doi.org/10.1016/j.actbio.2008.06.021.
[58] J. Victor, D. Van Doninck, L. Labey, B. Innocenti, P.M. Parizel, J. Bellemans, How precise can bony landmarks be determined on a CT scan of the knee? Knee 16 (5) (Oct. 2009) 358–365, https://doi.org/10.1016/j.knee.2009.01.001.
[59] G.N. Duda, K. Eckert-Hübner, R. Sokiranski, A. Kreutner, R. Miller, L. Claes, Analysis of inter-fragmentary movement as a function of musculoskeletal loading conditions in sheep, J. Biomech. 31 (3) (Dec. 1997) 201–210, https://doi.org/10.1016/S0021-9290(97)00127-9.
[60] Z.F. Lerner, B.C. Gadomski, A.K. Ipson, K.K. Haussler, C.M. Puttlitz, R.C. Browning, Modulating tibiofemoral contact force in the sheep hind limb via treadmill walking: predictions from an opensim musculoskeletal model, J. Orthop. Res. 33 (8) (2015) 1128–1133, https://doi.org/10.1002/jor.22829.
[61] E.C. Pegg, H.S. Gill, An open source software tool to assign the material properties of bone for ABAQUS finite element simulations, J. Biomech. 49 (13) (Sep. 2016) 3116–3121, https://doi.org/10.1016/j.jbiomech.2016.07.037.
[62] M. Berli, et al., Localized tissue mineralization regulated by bone remodelling: a computational approach, PLoS One 12 (3) (2017), e0173228, https://doi.org/10.1371/journal.pone.0173228. Mar.
[63] J.S. Lee, et al., Osteogenesis of 3D-printed PCL/TCP/bdECM scaffold using adipose-derived stem cells aggregates; an experimental study in the canine mandible, Int. J. Mol. Sci. 22 (11) (Jan. 2021), https://doi.org/10.3390/ijms22115409. Art. no. 11.
[64] F. Tabatabaei, A. Gelin, M. Rasoulianboroujeni, L. Tayebi, Coating of 3D printed PCL/TCP scaffolds using homogenized-fibrillated collagen, Colloids Surf. B Biointerfaces 217 (Sep. 2022), 112670, https://doi.org/10.1016/j.colsurfb.2022.112670.
[65] W.-F. Ho, A comparison of tensile properties and corrosion behavior of cast Ti–7.5Mo with c.p. Ti, Ti–15Mo and Ti–6Al–4V alloys, J. Alloys Compd. 464 (1) (Sep. 2008) 580–583, https://doi.org/10.1016/j.jallcom.2007.10.054.
[66] A. Bruyas, et al., Systematic characterization of 3D-printed PCL/β-TCP scaffolds for biomedical devices and bone tissue engineering: influence of composition and porosity, J. Mater. Res. 33 (14) (Jul. 2018) 1948–1959, https://doi.org/10.1557/jmr.2018.112.
[67] D.J. Kelly, P.J. Prendergast, Mechano-regulation of stem cell differentiation and tissue regeneration in osteochondral defects, J. Biomech. 38 (7) (Jul. 2005) 1413–1422, https://doi.org/10.1016/j.jbiomech.2004.06.026.
[68] P.-K. Juan, et al., Bioactivity and bone cell formation with poly-ε-caprolactone/bioceramic 3D porous scaffolds, Polymers 13 (16) (Jan. 2021), https://doi.org/10.3390/polym13162718. Art. no. 16.
[69] L.M. Lawrence, et al., Osteoregenerative potential of 3D-printed poly ε-caprolactone tissue scaffolds in vitro using minimally manipulative expansion of primary human bone marrow stem cells, Int. J. Mol. Sci. 24 (5) (Mar. 2023) 4940, https://doi.org/10.3390/ijms24054940.
[70] L. Zhang, B. Song, S.-K. Choi, Y. Shi, A topology strategy to reduce stress shielding of additively manufactured porous metallic biomaterials, Int. J. Mech. Sci. 197 (May 2021), 106331, https://doi.org/10.1016/j.ijmecsci.2021.106331.
[71] R. Owen, G.C. Reilly, In vitro models of bone remodelling and associated disorders, Front. Bioeng. Biotechnol. 6 (2018). Accessed: Mar. 27, 2023. [Online]. Available: https://www.frontiersin.org/articles/10.3389/fbioe.2018.00134.
[72] X. Feng, J.M. McDonald, Disorders of bone remodeling, Annu. Rev. Pathol. 6 (2011) 121–145, https://doi.org/10.1146/annurev-pathol-011110-130203.
[73] L. Geris, A. Gerisch, J.V. Sloten, R. Weiner, H.V. Oosterwyck, Angiogenesis in bone fracture healing: a bioregulatory model, J. Theor. Biol. 251 (1) (Mar. 2008) 137–158, https://doi.org/10.1016/j.jtbi.2007.11.008.
[74] L. Geris, K. Vandamme, I. Naert, J.V. Sloten, H. Van Oosterwyck, J. Duyck, Mechanical loading affects angiogenesis and osteogenesis in an in vivo bone chamber: a modeling study, Tissue Eng. 16 (11) (Nov. 2010) 3353–3361, https://doi.org/10.1089/ten.tea.2010.0130.